ACS Partner Journal

Journal of the American Society for Mass Spectrometry

pubs.acs.org/jasms

Research Article

Cyclic Ion Mobility Spectrometry Coupled to High-Resolution Time-of-Flight Mass Spectrometry Equipped with Atmospheric Solid Analysis Probe for the Molecular Characterization of Combustion Particulate Matter

Christopher P. Rüger,* Johann Le Maître, Eleanor Riches, Martin Palmer, Jürgen Orasche, Olli Sippula, Jorma Jokiniemi, Carlos Afonso, Pierre Giusti, and Ralf Zimmermann

Cite This: https://dx.doi.org/10.1021/jasms.0c00274

Read Online

ACCESS | Metrics & More | Article Recommendations | Supporting Information

ABSTRACT: Anthropogenic air pollution has a severe impact on climate and human health. The immense molecular complexity and diversity of particulate matter (PM) is a result of primary organic aerosol (POA) as well as secondary organic aerosols (SOAs). In this study, a direct inlet probe (DIP), i.e., atmospheric solids analysis probe (ASAP), with ion mobility high-resolution mass spectrometric detection is applied. Primary particulate matter emissions from three sources were investigated. Furthermore, photochemically aged emissions were analyzed. DIP introduction allowed for a direct analysis with almost no sample preparation and resulted in a complex molecular pattern. This pattern shifted through oxidation processes toward heavier species. For diesel emissions, the fuel's chemical characteristic is partially transferred to the particulate matter by incomplete combustion and characteristic alkylated series were found. Polycyclic aromatic hydrocarbons (PAHs) were identified as major contributors. Ion mobility analysis results in drift time profiles used for structural analysis. The apex position was used to prove structural changes, whereas the full-width-at-half-maximum was used to address the isomeric diversity. With this concept, the dominance of one or a few isomers for certain PAHs could be shown. In contrast, a broad isomeric diversity was found for oxygenated species. For the in-depth specification of fresh and aged spruce emissions, the ion mobility resolving power was almost doubled by allowing for three passes in the circular traveling wave design. The results prove that ASAP coupled with ion mobility spectrometry-mass spectrometry (IMS-MS) serves as a promising analytical approach for tackling the vast molecular complexity of PM.

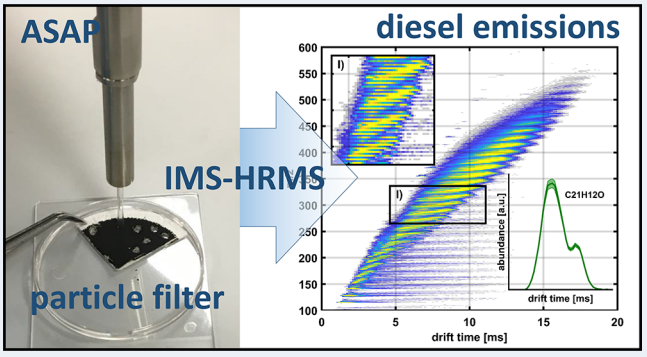

KEYWORDS: *cyclic ion mobility spectrometry, high-resolution mass spectrometry, direct inlet probe, particulate matter (PM), combustion emission, photochemical aerosol aging, complex mixtures*

INTRODUCTION

Anthropogenic air pollution exposes the environment to a complex mixture of gaseous or particulate organic pollutants, which severely impacts the climate and human health.[1−4] Combustion processes generate a major proportion of the ambient aerosol pollution.[1,2] The aerosol's particulate organic fraction includes primary organic aerosol (POA) particles as emitted from the source as well as secondary organic aerosols (SOAs) formed from gaseous emissions in the atmosphere due to photochemical and other processes. The chemical composition of combustion-derived particulate matter (PM) is tremendously complex with thousands known components.[5,6] Moreover, atmospheric aging and SOA formation alter and enlarge the chemical complexity even further.[7−10] These aging processes and SOA formation are commonly mimicked in laboratories by deploying large aerosol chambers (batch reactor)[11−13] or photochemical oxidation flow tube reactors.[14−17]

The chemical specification of these complex mixtures is an essential task for toxicological assessment and judging the potential impact on the climate.[2,18] For molecular level description, most often hyphenated chromatographic and mass spectrometric techniques are used.[19−21] Nonetheless, optimizing and running chromatographic techniques can be

Received: July 19, 2020
Revised: October 11, 2020
Accepted: November 18, 2020

time-consuming. Furthermore, gas chromatography is inherently limited in evaporation temperature and the accessible chemical space. In this respect, direct inlet probe (DIP) techniques have been proven to be a complementary approach for rapid complex mixture analysis, such as atmospheric pressure and reduced pressure solutions.[22−26]

For deciphering complex mixtures, resolving power is a prerequisite in analytical instrumentation.[27] For direct inlet probe approaches, without chromatographic separation capabilities, high-resolution mass analysis becomes even more important. In the last decades, Fourier-transform mass analyzers have delivered unbeaten resolving power and accuracy.[28] Nonetheless, in recent years, high-resolution time-of-flight instrumentation has improved drastically and modern orthogonal time-of-flight systems easily deliver resolving power above 50 000 fwhm.[29,30] With this, narrow mass splits can be differentiated. Limitations are still given by specific cases, such as the C_3/SH_4 3.4 mDa split.[23,29]

From high-resolution mass spectra, molecular formulas determination affords valuable but limited information on structural and functional aspects, such as the double bond equivalent (DBE).[31] Other structural features can be hypothesized on the basis of the heteroatoms, such as functional groups, but those attempts lack validation. Thus, the isomeric specification of complex mixtures directly from mass spectrometric response is not feasible. For this attempt, ion mobility spectrometry techniques coupled to high-resolution mass spectrometry have become frequently deployed.[32,33] They add an additional dimension of separation and extend the chemical information. In particular, trapped ion mobility, drift tube ion mobility, and traveling wave ion mobility devices can be employed.[32−36] From the ion mobility drift time profiles, the collision cross-section (CCS) can be calculated, an intrinsic property of ions directly related to their structure.[35] The resolution (CCS/ΔCCS) of state-of-the-art commercial ion mobility mass spectrometers is between 10 and 400.[32,37] Complex isomeric mixtures, such as those frequently found in petroleum analysis, cannot be resolved, and other peak parameters are used. In this context, the full-width-at-half-maximum (fwhm) was found to describe the isomeric diversity.[38,39]

Aside from a higher resolving power, a higher number of data points (bins) are beneficial for an accurate description of the IMS-profile of complex isomeric mixtures.[39−43] A very recent technology is cyclic ion mobility spectrometry (cIMS), allowing for the ions to pass multiple times in a circular traveling wave array, increasing the IMS resolving power by a factor of the square root of the pass number. In combination with an ion storage device before and after the cyclic array as well as with an option for collision-induced dissociation (CID), enormous flexibility is enabled for detailed molecular description.

In this proof-of-principle study, ion mobility spectrometry is applied for the first time with an atmospheric solid analysis probe (ASAP) for direct chemical characterization of particulate matter. Bruns et al. showed in 2010 the applicability of ASAP technology with solely mass spectrometric detection for laboratory-generated secondary organic aerosol and ambient PM.[44] The general aim is to enable a rapid molecular level description while at the same time overcoming tedious extraction procedures lowering the risk of contamination and artifacts. In the study of Bruns et al., characteristic precursors, such as α-pinene and isoprene, were used for ozonolysis and NO_3 oxidation.[44] In this presented study, primary combustion aerosols from a diesel generator and a logwood stove fired with wood and lignite are in focus. Moreover, the technique is evaluated for its capabilities of tracking molecular changes in aged emissions generated via an oxidation flow tube reactor, in particular by utilizing the IMS drift time profiles. As shown for synthetic polymers, the survey data can serve as chemical fingerprints.[45,46] We hypothesize that they are characteristic for the emissions source and type. Analysis of the fresh nonaged and aged emissions allows for an approach to monitor chemical transformation processes. The characterization currently is a very important topic as the aging of aerosols and SOA formation supposedly alters the toxicity of the aerosol.[47−49] The main objective is to reveal the analytical potential of IMS and high-resolution mass spectrometry (HRMS) for additional insights into the complex aerosol matrices, evaluate the discriminability of aerosols from different sources, and to recognize the impact of photochemical aging in complex emission aerosol. These objectives are addressed by retrieving molecular information from combining elemental composition attribution with the structure- and isomer-dependent IMS drift time profiles.

MATERIAL AND METHOD

Particulate Matter Samples. The investigated particulate matter samples were generated during a measurement campaign at the University of Eastern Finland in 2018. Briefly, diluted combustion aerosol (diesel 1:10, spruce/lignite 1:30) was sampled for up to 4 h with a flow of 10 L/min (2−2.4 m^3) on quartz fiber filter (QFF) directly from the emissions source or after passing through a novel high-volume photochemical emission aging flow tube reactor (PEAR), mimicking atmospheric aging reactions.[17] The subjects of this proof-of-principle study were fresh and aged PM emissions from a diesel generator (diesel fresh, diesel aged) and from a logwood stove feed with spruce (spruce fresh, spruce aged) as well as fresh emissions from lignite combustion. Information on the feed fuels can be found in Table S1.

Spruce logwood and lignite briquettes were burned in a modern nonheat-retaining chimney stove (Aduro 9.3, Denmark). The total combustion procedure for spruce logwood (*Picea abies*) took 4 h, including the sequential combustion of five batches of wood.[50] Lignite briquettes (Rekord, Lausitz Energie Bergbau AG) were burned after preparing the stove with two batches of spruce logwood, ensuring fast ignition (193 min sampling). Diesel combustion aerosol was generated with a diesel engine (KDE 6500 E, Kipor, 4.5 kW nominal power, 3000 min maximum speed, displacement 418 cm^{-3}) fueled with Finnish winter-grade ultralow sulfur diesel (EN590 diesel fuel). The engine was operated under different engine settings described elsewhere.[50]

Atmospheric aging was simulated in a photochemical emission aging flow tube reactor (PEAR)[17] operated with 254 nm UV-lamps with a photon flux of approximately 2×10^{16} photons cm^{-2} s^{-1}, relative humidity at room temperature of 50%, and externally fed with Ozone (9 ppm). The photochemical age can be estimated to be 2−3.5 days for logwood.[51,52] Despite considerable NO levels of approximately 2 ppm in the PEAR, aging can still be regarded as low-NOx conditions.[53]

Direct Inlet Probe Analysis. The aerosol particles were analyzed without any sample pretreatment directly from the QFF deploying a commercial atmospheric solid analysis probe

https://dx.doi.org/10.1021/jasms.0c00274
J. Am. Soc. Mass Spectrom. XXXX, XXX, XXX−XXX

(ASAP) from Waters Corporation, Wilmslow, UK. For this procedure, cleaned glass-capillaries (3 min heated at 350 °C within the ASAP source) were used. This ASAP approach can be regarded as thermal desorption atmospheric pressure chemical ionization (TD-APCI). The sample material is loaded to the glass-capillary by pressing the open side onto the brittle filter material (Figure S1). An aliquot of the material sticks within the capillary with the clean side facing below. This procedure ensures a slightly delayed evaporation in the ASAP source and leads to more reproducible experiments with a less pronounced spiking of the overall ion load. Details can be found elsewhere.[22] The loaded glass-capillary was mounted to the ASAP source. Molecular profile recording was started several seconds before injecting the material into the ionization volume. Analyses were performed at a probe temperature of 350 °C, minimizing the pyrolysis processes. Due to oxidation, ionization artifacts can occur in APCI;[54] the contamination of the ionization chamber with water and oxygen was minimized by only opening it for loading and unloading of the glass-capillary for several seconds. The high flow rate of pure nitrogen into the atmospheric pressure ionization source ensured minimum artifacts due to water and oxygen residues.

Ion Mobility Mass Spectrometric Analysis. The evaporated constituents from the particulate matter sample were ionized by atmospheric pressure chemical ionization (APCI) realized by a corona discharge needle held at 30 μA, and positive-mode spectra were recorded. Details of the instrumental design of the cyclic ion mobility spectrometer are described elsewhere.[55] Mass spectrometric detection from m/z 50−1000 was realized with an orthogonal time-of-flight system allowing spectra to be acquired with a resolution of over 70 000 fwhm. The cycle time (acquisition rate for the complete IMS-MS profile) was approximately 1 s, allowing several hundred individual scans during the runtime of the ASAP experiment to be registered. A web-based graphical user interface was used for instrument control and data acquisition.

Data Processing. The time- and mobility-resolved mass spectra were processed, deploying a self-developed Matlab-based graphical user interface (MATLAB R2018b).[56] The interface directly incorporates the Waters Corporation APIs for accessing the format of the raw data by implementing C++ routines. Each mass spectrum was recalibrated utilizing a specific list of manually proven signals. Mass spectrometric peaks are considered with an abundance of 100 au, roughly accounting for a signal-to-noise ratio of 6. Features (m/z versus drift time) were detected on the basis of a moving average approach along the ion mobility dimension.[39] Molecular formula attribution was performed within an error range of 10 ppm using the following boundaries: $C_{6-100}H_{6-200}N_{0-1}O_{010}S_{0-1}$; double bond equivalent (DBE) 0−20; m/z 100−1000; and H/C 0.4−2.8.

In the case of the lignite and diesel aerosol, homologue series were used for the elemental composition attribution to overcome the limitation concerning the mass spectrometric resolving power. In particular, C_3 versus SH_4 (Δ 3.4 mDa) for the lignite and C_3N versus H_2O_3 (Δ 2.7 mDa) for the diesel emission are problematic. Attribution at lower m/z with less mathematical and chemical possibilities allowed a differentiation. Nonetheless, the presented high-resolution time-of-flight mass spectrometric approach does not allow for an unambiguous assignment at higher m/z values. Despite this drawback, manual examination and the homologue series approach allowed for the attribution of over 90% of the total ion count.

RESULTS AND DISCUSSION

Evaluation and Molecular Information. First, the method and associated chemical characterization were evaluated with nonaged fresh diesel emissions. As shown in Figure 1a, a high total ion count (TIC) was immediately

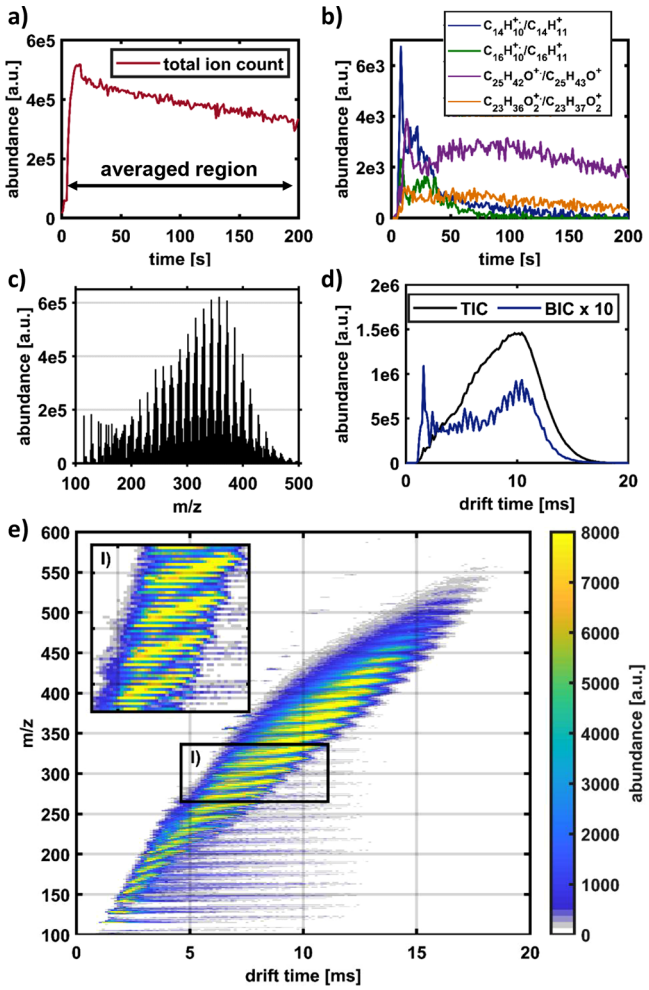

Figure 1. Exemplary results for nonaged fresh diesel combustion PM sample analyzed via ASAP-cIMS-MS. (a) Time-resolved total ion count (TIC), (b) time-resolved extracted ion counts of four evolved species, (c) average mass spectrum, (d) drift time-resolved total ion count and base peak ion count (BIC), and (e) survey view of the average m/z versus drift time data color-coded according to abundance, with an inset (I) highlighting the ion mobility separation and CH_2-homologue series.

received after inserting the loaded glass tube into the ionization chamber and lasted for several minutes. For the diesel sample with the highest organic matter loading on the QFF (engine emissions), up to 10 min of signal could be obtained, whereas, for the stove emissions (lignite/spruce), the signal declined more rapidly and vanished after 3−5 min. Figure 1b shows the emission behavior for selected species, two PAHs and two oxygenated compounds. Constituents with higher volatility, such as pure hydrocarbons (CH-class), are evaporated rapidly, whereas oxygenated species evolve with a delayed and more flat profile. This characteristic behavior related to the vapor

https://dx.doi.org/10.1021/jasms.0c00274
J. Am. Soc. Mass Spectrom. XXXX, XXX, XXX−XXX

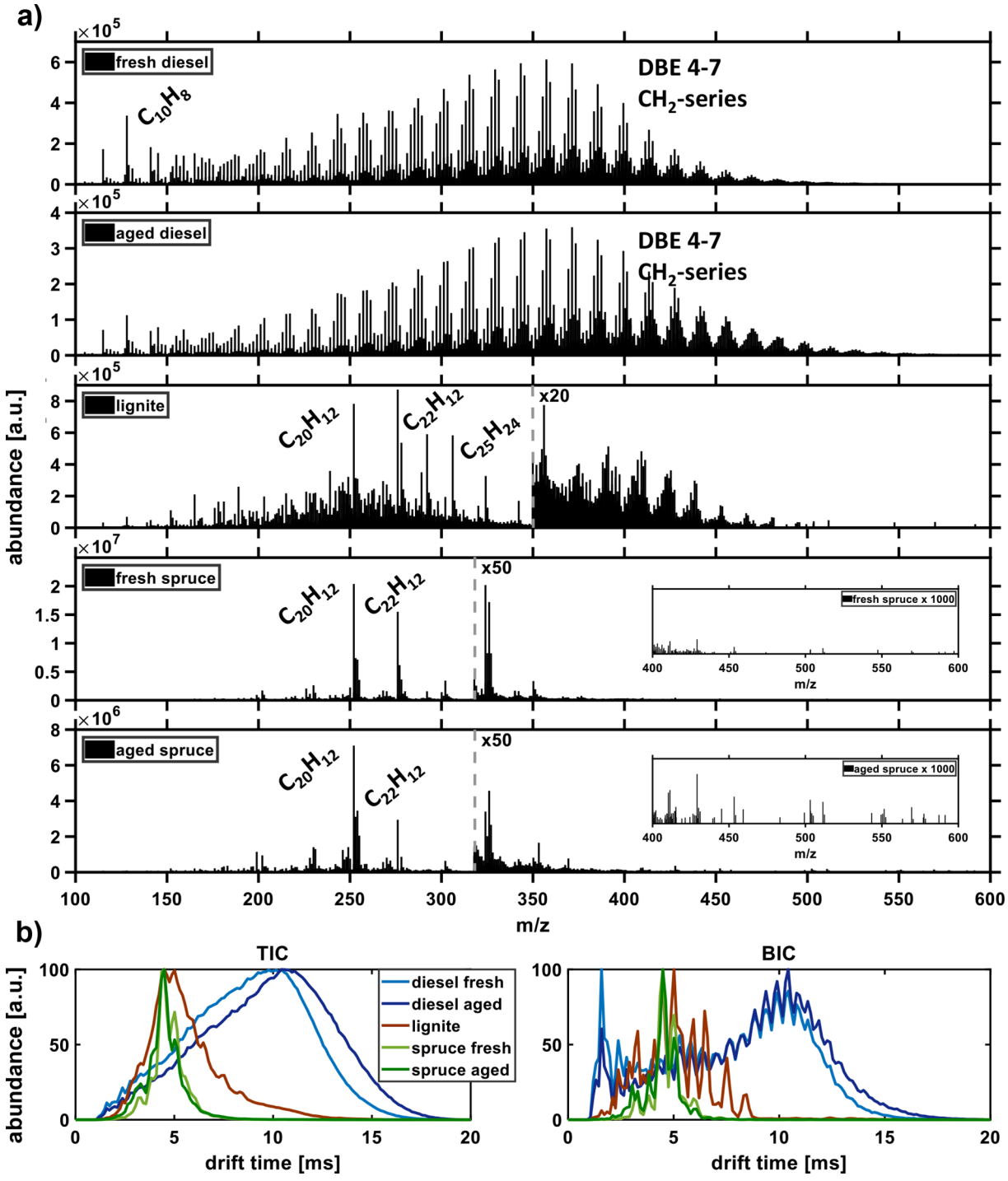

Figure 2. Comparison of the different aerosol sources and types investigated within this study. (a) Average mass spectrometric profile. The aged spruce revealed a slight increase of higher molecular weight species. (b) Overlaid drift time profiles of the ion mobility analyses (total ion count, TIC; base peak ion count, BIC).

pressure and boiling point of the components was previously reported in the literature.[22,23]

In the following, for processing and discussion, the region of evaporation was averaged and the mass spectrometric, as well as the ion mobility profile, were extracted. Figure 1c shows the average mass spectrum and Figure 1d shows the total and base peak ion count for the drift time information. For the diesel particulate matter, a very broad m/z range from m/z 100 up to almost m/z 700 is covered. Moreover, a tremendous structural diversity covering almost the complete drift time dimension was revealed. This drift time spread does not allow for increasing the pass number further as, otherwise, a wrap-around effect occurs with high mobility ions surpassing the low mobility ones. The diesel emissions are generated with commercial EN590 diesel fuel. This feed is mostly a distillate fraction of fossil fuel. In comprehensive petroleum analysis, so-called petroleomics, the structural and isomeric continuum is often referred to as Boduszynski continuum.[57−60] This continuum could also be found here for the diesel emission samples. This is in-line with previous findings that, despite

https://dx.doi.org/10.1021/jasms.0c00274
J. Am. Soc. Mass Spectrom. XXXX, XXX, XXX−XXX

combustion, the chemical characteristics are transferred from the fuel to the emitted particulate matter.[56,61] Moreover, this finding can be due to unburned constituents reported in the literature as a major contributor to engine emissions.[56,61,62] It should be noted that other aerosol sources can show drastically different profiles, which is discussed in detail below.

On the basis of the broad mass spectrometric profile, the heated nitrogen stream of the atmospheric analysis solid probe seems to allow for evaporation of heavy species prior to decomposition and far below the respective boiling point. This behavior was also found in the literature for direct inlet probe mass spectrometry of heavy petroleum fractions and is even more pronounced for reduced pressure direct inlet probe solutions.[23] The two-dimensional survey of m/z versus drift time (Figure 1e) summarizes these findings, and the ion mobility separation of repetitive building blocks can be seen. The high-resolution mass spectrometry detection (see Figure S2) allows for elemental composition attribution and the m/z difference of the building blocks belong to CH_2—units frequently found in petroleomics.[63] For the diesel emissions, over 50% of the abundance accounts for pure hydrocarbons (CH-class) followed by oxygenated species (CHO_{1-4}), whereas sulfur- and nitrogen-containing molecules were found with negligible intensity. Several alkylated series of CH-class species dominate the spectrum belonging to double bond equivalents of 4−7. Those series can be tentatively attributed to benzene and naphthenic derivatives. Naphthenic species dominate the lubrication oil used for operating the diesel engine, as revealed by supporting gas-chromatographic measurements (Figure S4). From the ASAP high-resolution mass spectrometry, it can be concluded that unburned or partially oxidized constituents of the lubrication oil contribute to the diesel emissions. Partially aromatic two−four ring derivatives are emitted. The critical role of unburned lubrication oil for aerosol emissions is also reported in the literature for other sources, such as marine diesel engines.[64,65]

Discrimination of Combustion Sources. Discriminating emission sources and understanding their emission characteristics on the molecular level are crucial. The three combustion aerosols can already be easily differentiated on the basis of the average mass spectrometric profile (Figure 2a). Diesel emissions show the broadest mass spectrometric profile, whereas the lignite aerosol revealed a less structured, i.e., less dominated by homologue series, mass spectrum with narrower distribution. This behavior is even more pronounced for the spruce emission, and the spectrum is dominated by few signals with a narrow spread in the m/z dimension. Concerning the ion mobility, Figure 2b shows the total ion count and base peak response, respectively. The same trend as for the mass spectrometric data can be found, with diesel aerosol exposing the broadest profile, lignite emissions as an intermediate, and spruce particulate matter with the narrowest ion mobility profile.

The model of an isomeric continuum, the so-called Boduszynski model,[59,60] can be deployed for a rough explanation of the isomeric diversity given by the ion mobility response of the aerosol sources. As stated above, diesel emissions are chemically linked to the fossil fuel feed and the isomeric continuum can also be found in the emission as the partial oxidation of the homologue series precursor or unburned residues. Lignite is an intermediate between wood as a fresh biomass and fossil fuel, aged millions of years under elevated temperature and pressure (anaerobic decomposition, maturation). Thus, the lignite emission shows a lower isomeric diversity than the diesel emissions but has a considerably broad profile. The spruce aerosol is chemically linked to wood biomass. The lignin matrix is structurally predefined on the basis of the biochemical formation processes. Consequently, the width of the ion mobility response, an estimate measure for the isomeric diversity, of spruce emission is comparatively low. Nonetheless, the combustion conditions will also play a role, and engine emissions (diesel) are drastically different from the stove (spruce/lignite) emissions.

Despite aging, both diesel aerosols, nonaged fresh and PEAR-aged emissions, revealed a comparable complexity with approximately 3000 attributed elemental compositions. Interestingly, smaller low-m/z constituents from all compound classes seem to be depleted for the aged emissions and an overall shift toward heavier and larger species can be seen (Figure 2). In the literature, even polymeric components were identified in atmospheric organic aerosols.[66] Nonetheless, the same elemental compositions from the aged and fresh emission from the CH-class and CHO-class show no significant change in the ion mobility profile. The variability of the ASAP method[22] and the comparable small changes for the diesel aerosol deploying PEAR aging hinder a more detailed applicative work here. In the following, the focus lies on the chemical comparison of the three emission sources.

Aside from the general profile discussed above (Figure 2), the diesel emissions also differ drastically on the molecular level from the lignite and spruce aerosol. Figure S3 visualizes the high-resolution mass spectrometric and ion mobility information as two-dimensional survey diagrams with the compound class distribution given as a pie plot inset. This allows for the rapid evaluation of the different sample types. The lignite shows a higher relative content of CHO_{1-3}-class constituents, whereas the spruce emissions are dominated by CH-class species and revealed higher oxygenated attributions (up to CHO_9). The lignite shows a more condensed response than the diesel emission, whereas the spruce combustion emission covers the narrowest chemical space. Figure S5 shows the mass spectrometric and ion mobility response for lignite emissions aged with the PEAR. In this case, the aging was conducted at an unrealistically high ozone concentration of several hundred parts per billion. Due to this rather untypical scenario, aged lignite emissions are not discussed in this study. Nonetheless, also for this sample material, distinct molecular profile changes can be seen and differentiated to the nonaged emissions.

High-resolution mass spectrometry for the description of complex mixtures utilizes specific diagrams, such as the carbon number versus DBE (showing exemplarily the CH-class) and van Krevelen diagrams (O/C versus H/C for CHO_x-class species). In Figure 3, these approaches are shown as modified versions incorporating the ion mobility response (apex peak position of the drift time profile) for color-coding. Ion mobility separates according to size and shape, which depends on the mass to a large extent. Consequently, the repetitive structure of the diesel chemical space given by alkylation revealed high drift times for species with a high carbon number. For a given carbon number, this dependence was found to be significantly lower along the DBE axes. This observation can be explained by the relatively compact aromatic structures compared to the flexible alkylated derivatives. For the lignite and spruce, this chemical space (DBE 0-8, #C 10-40) is almost empty. Moreover, it can be easily seen that the high aromatic (high

https://dx.doi.org/10.1021/jasms.0c00274
J. Am. Soc. Mass Spectrom. XXXX, XXX, XXX−XXX

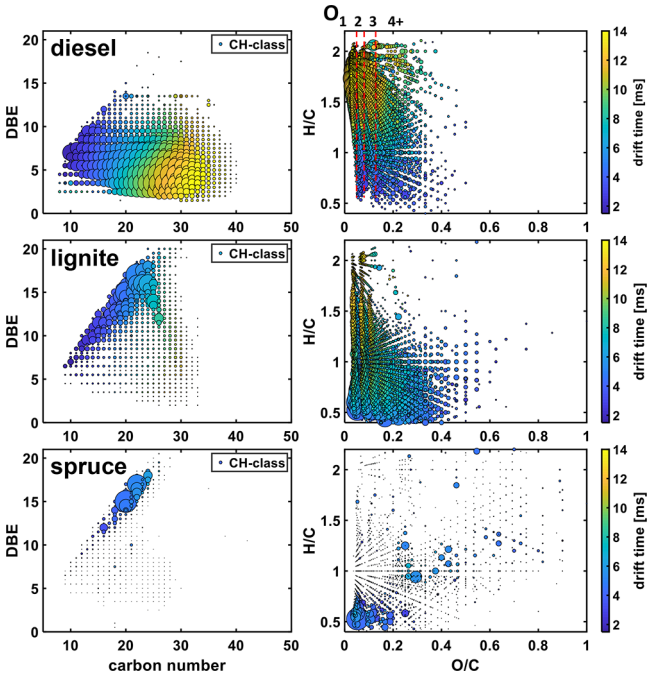

Figure 3. Molecular responses of the direct inlet probe approach given as carbon number versus DBE (left, CH-class) and Van-Krevelen diagrams (right, CHO_x-class) for the diesel, lignite, and spruce emissions. The apex peak position of the drift time (ion mobility response) is deployed for color-coding, whereas the size is coded according to the summed abundance of the respective elemental composition.

DBE) species of the lignite and spruce have comparable drift times. Those species are absent or only found with low abundance in the diesel emissions.

Regarding the modified van Krevelen diagram, it can be found that also the oxygenated constituents show higher aromaticity (low H/C) for the lignite and spruce emissions. For the spruce emissions, characteristics for biomass combustion aerosol, higher-oxygenated species were found. Lignite is dominated by compact (low drift time) species with high aromaticity. For the diesel emissions, the different oxygenated classes (CHO_{1-4}) can be seen as clusters of signals with narrow O/C (horizontal) and broader H/C spread (vertical). Interestingly, those clusters (oxygenated classes) show the same drift time spread, i.e., higher oxygenated species with comparable H/C have comparable drift times. This finding indicates that the structural continuum can also be found across the oxygenated classes. The complex molecular profile given by the atmospheric solid analysis probe can be, thus, extended by structural information from the drift time profiles.

More targeted information was obtained by the comparison of the extracted drift time profiles of the three emission sources for the individual molecular formulas. Polycyclic aromatic hydrocarbons (PAHs) are comprehensively studied in combustion aerosol and will serve as targets here.[67−69] Despite the nonalkylated PAHs with more than 5-rings, such as napthofluoranthene/pyrene ($C_{24}H_{14}$), which are absent in the diesel emissions, a majority of the investigated 2−5-ring PAHs can be found in all three samples. Other species, such as $C_{20}H_{14}$, most likely a binaphthalene, were only found in the diesel sample.

Interestingly, for most of the investigated PAHs, the drift time profiles are almost identical between the emission sources (Figure 4), and a narrow symmetrical unimodal Gaussian distribution indicating a single isomer or a continuum of isomers very close in structure could be found. Besides, the full-width-at-half-maximum (fwhm), a measure for the isomeric diversity,[38] is identical for those targets. For $C_{14}H_{10}$, anthracene or phenanthrene, a dominant signal with a small shoulder can be found. In combustion aerosol, phenanthrene was reported to be the dominant species. This is in agreement with the lower drift time (smaller and more compact species) signal being the dominant peak. The fwhm for the phenanthrene peak is approximately 0.3 ms, almost the same fwhm as that for the one dominant $C_{18}H_{12}$ peak, leading to the conclusion of one dominant isomer, most likely chrysene. For $C_{20}H_{12}$ and $C_{22}H_{12}$, the fwhm is significantly larger and several PAH structures can be expected. Regarding the oxygenated species, the attribution $C_{18}H_8O_3$ could chemically result in various isomers but the drift time profile shows the same position and shape for all three samples. Most likely accounting for structurally close isomers of 5-ring oxa-dione PAHs, such as 4-oxa-benzo[*cd*]pyrene-3,5-dione, reported in the literature.[70] The same can be found for $C_{17}H_{10}O$, most likely benzanthrone, and $C_{16}H_{10}O$, tentatively a hydroxypyrene.

Also, other cases with different apex peak positions or different fwhm values could be found. Selected examples with a higher m/z can also be found in Figure 4. Briefly, $C_{19}H_{32}O_1$, giving a sharp peak at a lower drift time for lignite and spruce and a broad signal at higher drift times for the diesel emission, could be a rigid sterane (spruce/lignite) or highly alkylated oxygenated aromatic derivatives (diesel), respectively. $C_{19}H_{25}O_2$ shows the same apex peak position and could be an ester but was found to be less isomerically diverse for the spruce emissions and broadest for the diesel with lignite in between. The same trend is true for the respective ketone/aldehyde ($C_{19}H_{25}O_1$). For $C_{21}H_{17}$, most likely a 4-ring PAH, spruce shows more compact species with two peaks visible in the drift time profile, whereas lignite and diesel reveal an unimodal peak shape. The CHO_2-class signal $C_{19}H_{17}O_2$ revealed a multimodal peak shape with at least three peaks for the spruce. Those peaks could be groups of structurally similar isomers with the same core structure. For the emissions with fossil feed (diesel and lignite), a single peak was found. In this case, the biomass-related emission seems to be structurally more diverse.

Concerning environmental health, many PAHs and their oxygenated derivatives are reported to be mutagenic and carcinogenic.[71,72] Thus, ASAP-IMS-MS, as a rapid molecularly resolved screening technology, can help for the toxicological assessment of a high number of PM samples with minimized pretreatment.

Effect of Photochemical Aging. In this last section, the retrieved chemical profiles of the fresh and PEAR-aged spruce particulate matter will be compared to evaluate the reproducibility in more detail and the capabilities for differentiating aerosol samples with a close chemical profile. Here, the unique characteristic of the cyclic ion mobility spectrometer was utilized. Passing the ions more than one turn in the circular traveling wave array could lead to a wrap-around effect, i.e., fast low-collision-cross-section ions surpassing the slow high-collision-cross-section ions. The resulting data cannot be deconvoluted and hardly utilized for chemical characterization. For overcoming this limitation, the isomeric

https://dx.doi.org/10.1021/jasms.0c00274
J. Am. Soc. Mass Spectrom. XXXX, XXX, XXX−XXX

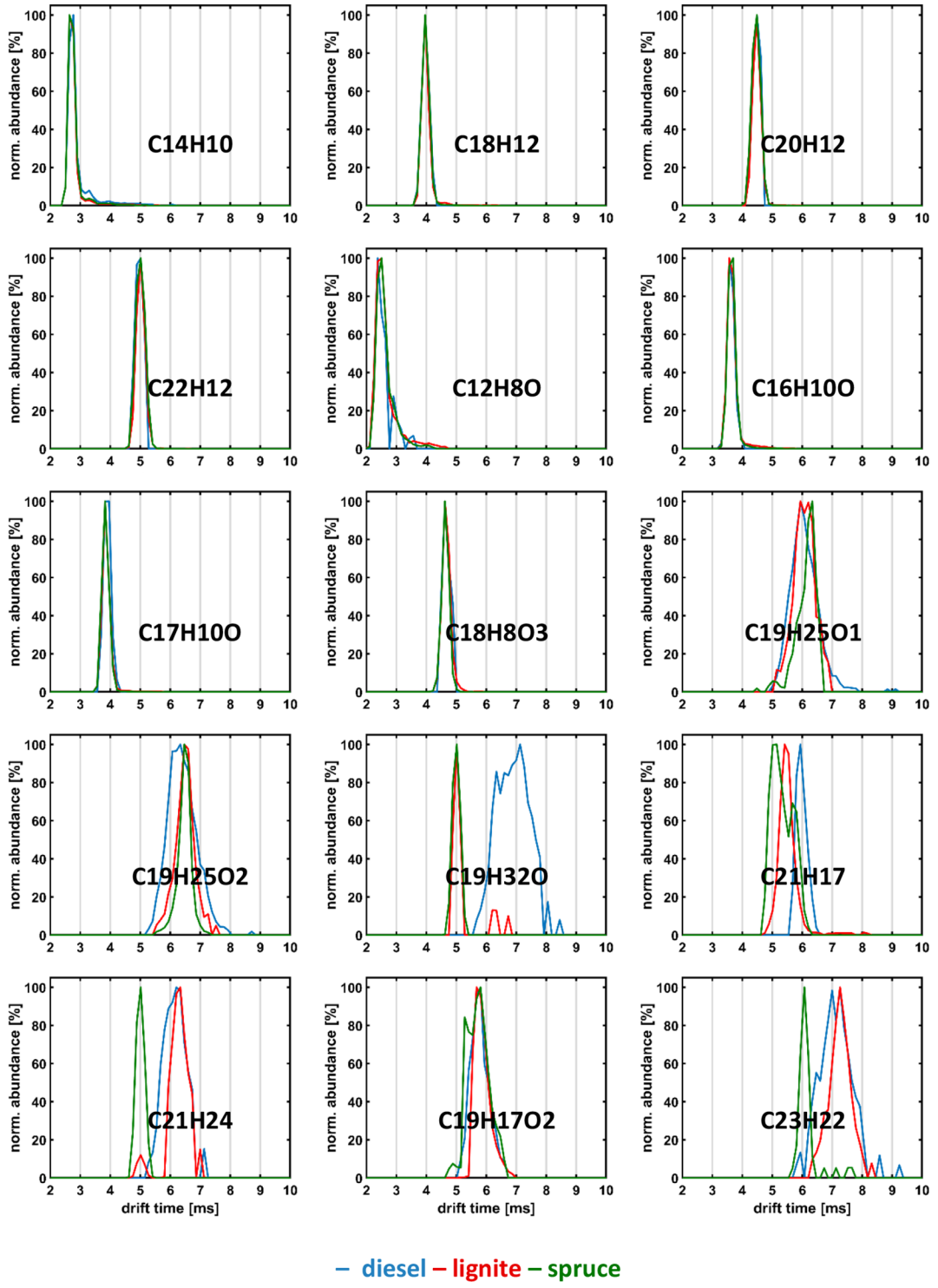

Figure 4. Targeted comparison of PAHs and selected CHO_x-class ion mobility spectra and for the nonaged fresh diesel (blue), the lignite (red), and nonaged fresh spruce (green). Three general characteristics could be found: (1) identical peak positions and comparable fwhm, (2) different fwhm, and (3) different peak apex positions of the drift time profile.

spread was limited by quadrupole m/z selection prior to ion mobility separation to a range of m/z 250 ± 50 (QcIMS). Consequently, three passes were taken for the ion mobility separation. This straightforward and uncomplicated adjustment immediately increased the ion mobility resolving power by a factor of roughly 1.8 to over 100. Furthermore, the increased pass number for a narrow mass window will drastically increase the number of data points of the ion mobility spectra. fwhm and other peak parameters can potentially be determined with a higher accuracy (Figures S6 and S7).

The molecular complexity, by means of the number of mass spectrometric signals and attributed elemental compositions, increased slightly about 10−50 attributions for the PEAR-aged spruce emission. On the basis of the mean values of the triplicate QcIMS experiments, a very low variation of below 7%

https://dx.doi.org/10.1021/jasms.0c00274
J. Am. Soc. Mass Spectrom. XXXX, XXX, XXX−XXX

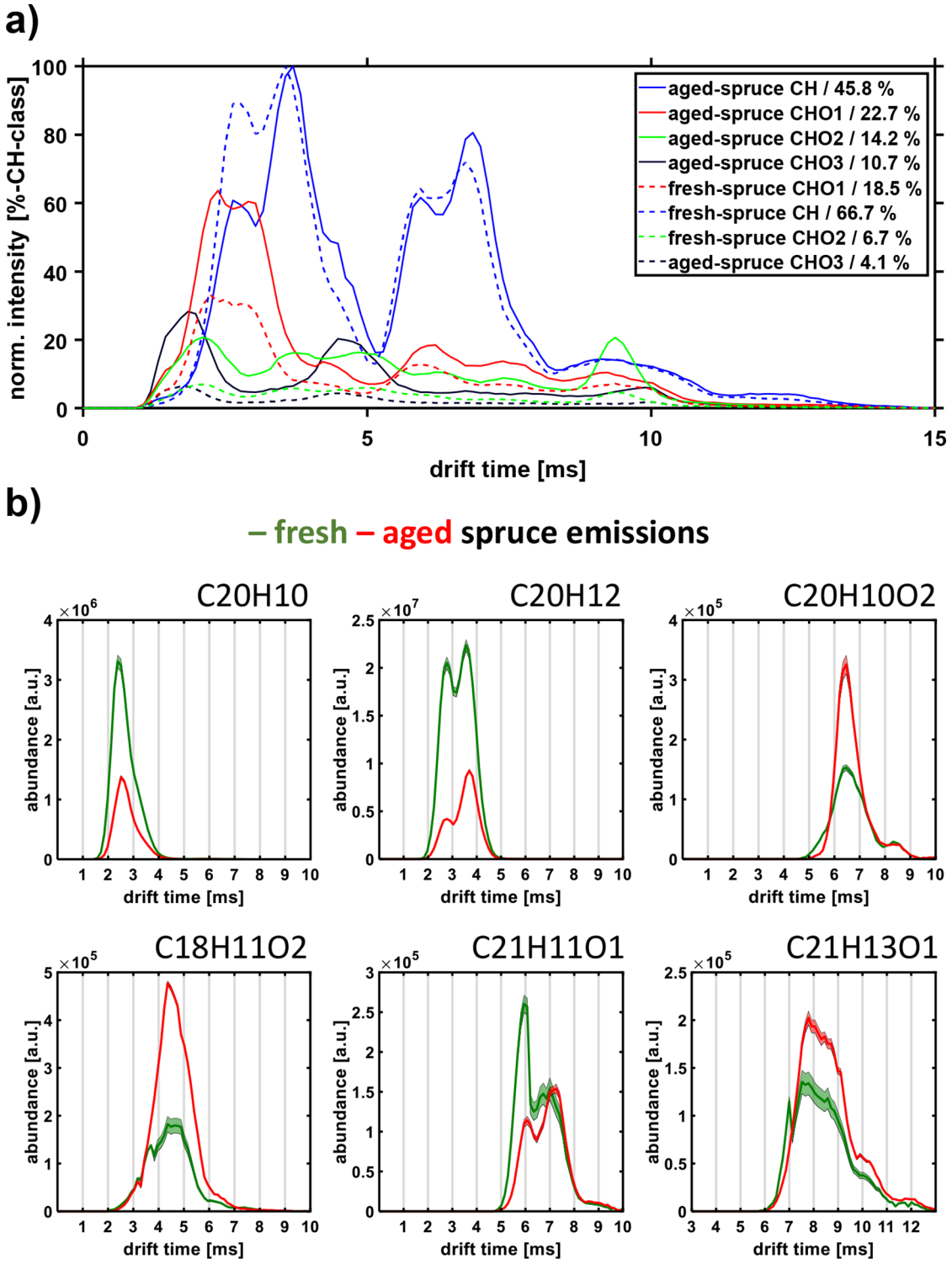

Figure 5. Grouped and individual drift time profiles for fresh and aged spruce molecular profiles. (a) Compound class drift time profile for the CH-class and oxygenated species (O_{1-3}). (b) Selected drift time profiles based on species found in fresh and aged spruce emissions with the difference in abundance.

in the number of attributions was found. The absolute abundance along the ASAP time-profile was found to be less reproducible, and a variation of up to 30% was revealed. Various factors can lead to this variation for DIP-MS analysis.[22] Thus, absolute abundance is not the best descriptor here for a comparison. Hence, it will be focused on the occurrence of chemical formulas, the TIC-normalized and relative abundance, and their respective drift time profiles.

The photochemical aging leads to a shift in the chemical space, and higher oxygenated species were found with increased abundance (Figure S8). Interestingly the aromaticity (hydrogen deficiency, H/C) is only slightly affected with a slight decrease, and a horizontal shift in the Van Krevelen

https://dx.doi.org/10.1021/jasms.0c00274
J. Am. Soc. Mass Spectrom. XXXX, XXX, XXX−XXX

diagram can be found. The decrease in H/C with increasing O/C is also reported in the literature for aging of wood combustion emissions.[73] Thus, oxygen is most likely added in a low degree to the precursor as aldehydes and ketones in the first steps. Also, the formation of carboxylic acids is well described in the literature.[73] Consequently, van Krevelen diagrams serve as an ideal tool for fingerprinting and showing the overall change, but individual drift time profiles are needed for molecular level discussion.

Figure 5a shows the summed drift time profiles for formulas belonging to the same compound class. The increase of the relative abundance (data normalized to the CH-class) of CHO_x-class species can be seen. Moreover, each class shows the same general behavior for the fresh and aged emissions, but the abundance varies. For the CH-species of the aged emissions, the abundance of smaller species declines and oxygenated classes show lower drift times. As stated for the adapted van Krevelen fingerprint incorporating the apex of the drift time profile, the PEAR aging does not lead to a complete change in the chemical profile but a clear shift toward higher oxygenated species was observed.

Figure 5b exemplarily shows drift time profiles for the aged and fresh emissions in all three replicates with relatively high abundance. For specific signals, such as the $C_{20}H_{10}$, only the abundance is affected. For other species, such as $C_{20}H_{12}$, the overall width, shape, and number of peaks remain but the abundance of certain peaks changes. $C_{20}H_{12}$, most likely 4−5-ring PAHs, such as benzo[*a*]pyrene and perylene, was discussed before. We see a slight separation for these ions with three passes, and two groups of isomers can be identified. This is caused by the increased number of passes in the cyclic ion mobility device, enabling a higher resolving power and a higher number of sampling points (bins) along a drift time peak. Consequently, the ion mobility spectra can be described with higher accuracy. In this case, the smaller, more compact feature with a lower drift time declined significantly during the aging. Certain oxygenated species also drop in abundance, such as $C_{21}H_{11}O_1$, tentatively assigned as an oxygenated 6-ring aromatic. Highly oxidized aromatics resulted from the aerosol aging are most likely not detectable with the heated probe due to thermal decomposition or low vapor pressure.

The ASAP approach will be limited by the volatility and stability of the constituents, which is particularly important for aged and/or biomass-combustion aerosols. Higher oxygenated species might account for a larger proportion of the chemical profile as direct infusion investigations of aerosols extracts suggest. Nonetheless, the presented approach rapidly revealed molecular fingerprints of emissions with comparable chemical space and distinct changes as well as similarities on the molecular level. Unlike in the previous study of Bruns et al.,[44] where SOA newly formed from gas phase or ambient PM was investigated, the photochemical aging of real emission results in significantly altered spectra dominated by primary emission compounds. In this regard, highly oxygenated SOA species might not be entirely reflected by this thermal desorption approach, but certain chemical transformations can be monitored. Nonetheless, the comparison of fresh and aged aerosols from the same source is a preferable experimental setting, as the matrix effects are very much comparable in both cases.

CONCLUSION

Atmospheric solid analysis probe (ASAP), together with ion mobility separation and high-resolution mass spectrometric detection (IMS-MS), allowed for a rapid chemical characterization of combustion aerosols with almost no sample preparation. It was shown that the approach serves as a fingerprinting technique. Aerosol emission sources and types (aged versus nonaged) can be distinguished on the basis of the IMS-MS survey data.

The concept of an isomeric continuum used in petroleomics (Boduszynski continuum) was deployed on the basis of the attributed elemental compositions. Engine emitted aerosol (diesel emissions) and stove emissions (lignite/spruce) revealed different levels of this continuum with diesel emissions > lignite emissions > spruce emissions. Moreover, classical fingerprinting visualization techniques, such as DBE versus carbon number and van Krevelen diagrams, can be successfully extended by incorporating the structural information on the drift time profiles.

The capability of the method to address samples closely related in chemistry was shown by the comparison of fresh and nonaged spruce aerosol samples. Distinct differences were found for the mass spectrometric response and the drift time profiles. A clear shift toward higher oxygenated species was revealed. The drift time profiles gave valuable structural information showing a shift toward larger isomers.

In conclusion, the method allows for a straightforward classification of real-world particulate matter. Important molecular species such as PAHs and oxygenated PAHs can be monitored. We were able to reveal specific structural differences at the molecular level. Thus, the authors believe that ASAP-IMS-MS, as a rapid molecularly resolved screening technology, can help with the toxicological assessment of a high number of PM samples with minimized pretreatment.

Future studies will focus on modeling and theoretical calculations of structures on the basis of the drift time profiles. In combination with direct infusion experiments or hyphenated solutions, chemical characterization will be allowed on the structural level. This information will be utilized for challenges in environmental health and climate change research.

ASSOCIATED CONTENT

Supporting Information

The Supporting Information is available free of charge at https://pubs.acs.org/doi/10.1021/jasms.0c00274.

Table of information on the feed fuels and figures of photographic description of the particulate matter sampling, high-resolution mass spectrum, survey of the ion mobility and mass spectrometric response, screening of lubrication oil, total ion count drift time profile, direct comparison of the drift time profile for the extracted ion mobilogram, and Van Krevelen diagrams (PDF)

AUTHOR INFORMATION

Corresponding Author

Christopher P. Rüger − *Joint Mass Spectrometry Centre/ Chair of Analytical Chemistry, University of Rostock, 18059 Rostock, Germany; International Joint Laboratory−iC2MC: Complex Matrices Molecular Characterization, Total Research and Technology Gonfreville (TRTG), 76700 Harfleur, France;* orcid.org/0000-0001-9634-9239; Email: christopher.rueger@uni-rostock.de

https://dx.doi.org/10.1021/jasms.0c00274
J. Am. Soc. Mass Spectrom. XXXX, XXX, XXX−XXX

Authors

Johann Le Maître − *International Joint Laboratory−iC2MC: Complex Matrices Molecular Characterization, Total Research and Technology Gonfreville (TRTG), 76700 Harfleur, France; TOTAL Refining and Chemicals, 76700 Harfleur, France*

Eleanor Riches − *Waters Corporation, SK9 4AX Wilmslow, United Kingdom;* orcid.org/0000-0003-4218-1703

Martin Palmer − *Waters Corporation, SK9 4AX Wilmslow, United Kingdom;* orcid.org/0000-0003-1658-9334

Jürgen Orasche − *Joint Mass Spectrometry Centre (JMSC)/ Helmholtz Zentrum München, Comprehensive Molecular Analytics, 85764 Neuherberg, Germany*

Olli Sippula − *University of Eastern Finland, 70211 Kuopio, Finland*

Jorma Jokiniemi − *University of Eastern Finland, 70211 Kuopio, Finland*

Carlos Afonso − *International Joint Laboratory−iC2MC: Complex Matrices Molecular Characterization, Total Research and Technology Gonfreville (TRTG), 76700 Harfleur, France; Normandie Université, COBRA, UMR 6014 et FR 3038, Université de Rouen-Normandie, 76130 Mont Saint Aignan, France;* orcid.org/0000-0002-2406-5664

Pierre Giusti − *International Joint Laboratory−iC2MC: Complex Matrices Molecular Characterization, Total Research and Technology Gonfreville (TRTG), 76700 Harfleur, France; TOTAL Refining and Chemicals, 76700 Harfleur, France;* orcid.org/0000-0002-9569-3158

Ralf Zimmermann − *Joint Mass Spectrometry Centre/Chair of Analytical Chemistry, University of Rostock, 18059 Rostock, Germany; Joint Mass Spectrometry Centre (JMSC)/ Helmholtz Zentrum München, Comprehensive Molecular Analytics, 85764 Neuherberg, Germany*

Complete contact information is available at: https://pubs.acs.org/10.1021/jasms.0c00274

Notes

The authors declare no competing financial interest.

■ ACKNOWLEDGMENTS

The aerosols investigated in this work have been generated in the framework of the HICE virtual Helmholtz Institute (www.hice-vi.eu) during a measurements campaign at the ILMARI aerosol facility at the University of Eastern Finland. The analysis was performed as a method feasibility test in the framework of the Helmholtz International Lab. aeroHEALTH (www.aerohealth.eu).

■ REFERENCES

(1) Di, Q.; Wang, Y.; Zanobetti, A.; Wang, Y.; Koutrakis, P.; Choirat, C.; Dominici, F.; Schwartz, J. D. Air Pollution and Mortality in the Medicare Population. *N. Engl. J. Med.* **2017**, *376*, 2513.

(2) Allen, M. R. *Climate change 2014: Synthesis report*; IPCC: Geneva, Switzerland, 2015.

(3) Pachauri, R. K. *Climate change 2007: Synthesis Report*; IPCC: Geneva, Switzerland, 2008.

(4) Corbett, J. J.; Winebrake, J. J.; Green, E. H.; Kasibhatla, P.; Eyring, V.; Lauer, A. Mortality from ship emissions: A global assessment. *Environ. Sci. Technol.* **2007**, *41* (24), 8512−8518.

(5) Rogge, W. F.; Hildemann, L. M.; Mazurek, M. A.; Cass, G. R.; Simoneit, B. R. T. Sources of fine organic aerosol. 2. Noncatalyst and catalyst-equipped automobiles and heavy-duty diesel trucks. *Environ. Sci. Technol.* **1993**, *27* (4), 636−651.

(6) Rogge, W. F.; Hildemann, L. M.; Mazurek, M. A.; Cass, G. R.; Simoneit, B. R. T. Sources of fine organic aerosol. 3. Road dust, tire debris, and organometallic brake lining dust: roads as sources and sinks. *Environ. Sci. Technol.* **1993**, *27* (9), 1892−1904.

(7) Hallquist, M.; Wenger, J. C.; Baltensperger, U.; Rudich, Y.; Simpson, D.; Claeys, M.; Dommen, J.; Donahue, N. M.; George, C.; Goldstein, A. H.; Hamilton, J. F.; Herrmann, H.; Hoffmann, T.; Iinuma, Y.; Jang, M.; Jenkin, M. E.; Jimenez, J. L.; Kiendler-Scharr, A.; Maenhaut, W.; McFiggans, G.; Mentel, T. F.; Monod, A.; Prévôt, A. S. H.; Seinfeld, J. H.; Surratt, J. D.; Szmigielski, R.; Wildt, J. The formation, properties and impact of secondary organic aerosol: current and emerging issues. *Atmos. Chem. Phys.* **2009**, *9*, 5155−5236.

(8) Jimenez, J. L.; Canagaratna, M. R.; Donahue, N. M.; Prevot, A. S. H.; Zhang, Q.; Kroll, J. H.; DeCarlo, P. F.; Allan, J. D.; Coe, H.; Ng, N. L.; Aiken, A. C.; Docherty, K. S.; Ulbrich, I. M.; Grieshop, A. P.; Robinson, A. L.; Duplissy, J.; Smith, J. D.; Wilson, K. R.; Lanz, V. A.; Hueglin, C.; Sun, Y. L.; Tian, J.; Laaksonen, A.; Raatikainen, T.; Rautiainen, J.; Vaattovaara, P.; Ehn, M.; Kulmala, M.; Tomlinson, J. M.; Collins, D. R.; Cubison, M. J.; Dunlea, E. J.; Huffman, J. A.; Onasch, T. B.; Alfarra, M. R.; Williams, P. I.; Bower, K.; Kondo, Y.; Schneider, J.; Drewnick, F.; Borrmann, S.; Weimer, S.; Demerjian, K.; Salcedo, D.; Cottrell, L.; Griffin, R.; Takami, A.; Miyoshi, T.; Hatakeyama, S.; Shimono, A.; Sun, J. Y.; Zhang, Y. M.; Dzepina, K.; Kimmel, J. R.; Sueper, D.; Jayne, J. T.; Herndon, S. C.; Trimborn, A. M.; Williams, L. R.; Wood, E. C.; Middlebrook, A. M.; Kolb, C. E.; Baltensperger, U.; Worsnop, D. R. Evolution of organic aerosols in the atmosphere. *Science* **2009**, *326*, 1525−1529.

(9) Atkinson, R.; Arey, J. Atmospheric degradation of volatile organic compounds. *Chem. Rev.* **2003**, *103*, 4605−4638.

(10) Kroll, J. H.; Donahue, N. M.; Jimenez, J. L.; Kessler, S. H.; Canagaratna, M. R.; Wilson, K. R.; Altieri, K. E.; Mazzoleni, L. R.; Wozniak, A. S.; Bluhm, H.; Mysak, E. R.; Smith, J. D.; Kolb, C. E.; Worsnop, D. R. Carbon oxidation state as a metric for describing the chemistry of atmospheric organic aerosol. *Nat. Chem.* **2011**, *3*, 133−139.

(11) Chirico, R.; DeCarlo, P. F.; Heringa, M. F.; Tritscher, T.; Richter, R.; Prévôt, A. S. H.; Dommen, J.; Weingartner, E.; Wehrle, G.; Gysel, M.; Laborde, M.; Baltensperger, U. Impact of aftertreatment devices on primary emissions and secondary organic aerosol formation potential from in-use diesel vehicles: results from smog chamber experiments. *Atmos. Chem. Phys.* **2010**, *10*, 11545−11563.

(12) Chu, B.; Liggio, J.; Liu, Y.; He, H.; Takekawa, H.; Li, S.-M.; Hao, J. Influence of metal-mediated aerosol-phase oxidation on secondary organic aerosol formation from the ozonolysis and OH-oxidation of α-pinene. *Sci. Rep.* **2017**, *7*, 40311.

(13) Tiitta, P.; Leskinen, A.; Hao, L.; Yli-Pirilä, P.; Kortelainen, M.; Grigonyte, J.; Tissari, J.; Lamberg, H.; Hartikainen, A.; Kuuspalo, K.; Kortelainen, A.-M.; Virtanen, A.; Lehtinen, K. E. J.; Komppula, M.; Pieber, S.; Prévôt, A. S. H.; Onasch, T. B.; Worsnop, D. R.; Czech, H.; Zimmermann, R.; Jokiniemi, J.; Sippula, O. Transformation of logwood combustion emissions in a smog chamber: formation of secondary organic aerosol and changes in the primary organic aerosol upon daytime and nighttime aging. *Atmos. Chem. Phys.* **2016**, *16*, 13251−13269.

(14) Ahlberg, E.; Falk, J.; Eriksson, A.; Holst, T.; Brune, W. H.; Kristensson, A.; Roldin, P.; Svenningsson, B. Secondary organic aerosol from VOC mixtures in an oxidation flow reactor. *Atmos. Environ.* **2017**, *161*, 210−220.

(15) Jathar, S. H.; Friedman, B.; Galang, A. A.; Link, M. F.; Brophy, P.; Volckens, J.; Eluri, S.; Farmer, D. K. Linking Load, Fuel, and Emission Controls to Photochemical Production of Secondary Organic Aerosol from a Diesel Engine. *Environ. Sci. Technol.* **2017**, *51*, 1377−1386.

(16) Ortega, A. M.; Day, D. A.; Cubison, M. J.; Brune, W. H.; Bon, D.; de Gouw, J. A.; Jimenez, J. L. Secondary organic aerosol formation and primary organic aerosol oxidation from biomass-burning smoke in a flow reactor during FLAME-3. *Atmos. Chem. Phys.* **2013**, *13*, 11551−11571.

(17) Ihalainen, M.; Tiitta, P.; Czech, H.; Yli-Pirilä, P.; Hartikainen, A.; Kortelainen, M.; Tissari, J.; Stengel, B.; Sklorz, M.; Suhonen, H.; Lamberg, H.; Leskinen, A.; Kiendler-Scharr, A.; Harndorf, H.; Zimmermann, R.; Jokiniemi, J.; Sippula, O. A novel high-volume Photochemical Emission Aging flow tube Reactor (PEAR). *Aerosol Sci. Technol.* **2019**, *53*, 276−294.
(18) *Ambient Air Pollution: A global Assessment of Exposure and Burden of Disease*; World Health Organization, 2016.
(19) Alam, M. S.; Harrison, R. M. Recent advances in the application of 2-dimensional gas chromatography with soft and hard ionisation time-of-flight mass spectrometry in environmental analysis. *Chem. Sci.* **2016**, *7*, 3968−3977.
(20) Oros, D. R.; Simoneit, B. R. T. Identification of Molecular Tracers in Organic Aerosols from Temperate Climate Vegetation Subjected to Biomass Burning. *Aerosol Sci. Technol.* **1999**, *31*, 433−445.
(21) Weggler, B. A.; Ly-Verdu, S.; Jennerwein, M.; Sippula, O.; Reda, A. A.; Orasche, J.; Gröger, T.; Jokiniemi, J.; Zimmermann, R. Untargeted Identification of Wood Type-Specific Markers in Particulate Matter from Wood Combustion. *Environ. Sci. Technol.* **2016**, *50*, 10073−10081.
(22) Castilla, C.; Rüger, C. P.; Marcotte, S.; Lavanant, H.; Afonso, C. Direct Inlet Probe Atmospheric Pressure Photo and Chemical Ionization Coupled to Ultrahigh Resolution Mass Spectrometry for the Description of Lignocellulosic Biomass. *J. Am. Soc. Mass Spectrom.* **2020**, *31*, 822−831.
(23) Käfer, U.; Gröger, T.; Rüger, C. P.; Czech, H.; Saraji-Bozorgzad, M.; Wilharm, T.; Zimmermann, R. Direct inlet probe - High-resolution time-of-flight mass spectrometry as fast technique for the chemical description of complex high-boiling samples. *Talanta* **2019**, *202*, 308−316.
(24) Barrère, C.; Hubert-Roux, M.; Afonso, C.; Racaud, A. Rapid analysis of lubricants by atmospheric solid analysis probe-ion mobility mass spectrometry. *J. Mass Spectrom.* **2014**, *49*, 709−715.
(25) Käfer, U.; Gröger, T.; Rohbogner, C. J.; Struckmeier, D.; Saraji-Bozorgzad, M. R.; Wilharm, T.; Zimmermann, R. Detailed Chemical Characterization of Bunker Fuels by High-Resolution Time-of-Flight Mass Spectrometry Hyphenated to GC × GC and Thermal Analysis. *Energy Fuels* **2019**, *33*, 10745.
(26) Ballesteros-Gómez, A.; Brandsma, S. H.; de Boer, J.; Leonards, P. E. G. Direct probe atmospheric pressure photoionization/atmospheric pressure chemical ionization high-resolution mass spectrometry for fast screening of flame retardants and plasticizers in products and waste. *Anal. Bioanal. Chem.* **2014**, *406*, 2503.
(27) Marshall, A. G.; Blakney, G. T.; Beu, S. C.; Hendrickson, C. L.; McKenna, A. M.; Purcell, J. M.; Rodgers, R. P.; Xian, F. Petroleomics: a test bed for ultra-high-resolution Fourier transform ion cyclotron resonance mass spectrometry. *Eur. J. Mass Spectrom.* **2010**, *16*, 367−371.
(28) Schmitt-Kopplin, P.; Kanawati, B. *Fundamentals and Applications of Fourier Transform Mass Spectrometry*; Elsevier: San Diego, CA, 2019.
(29) Byer, J. D.; Siek, K.; Jobst, K. Distinguishing the C3 vs SH4Mass Split by Comprehensive Two-Dimensional Gas Chromatography-High Resolution Time-of-Flight Mass Spectrometry. *Anal. Chem.* **2016**, *88*, 6101.
(30) Gröger, T. M.; Käfer, U.; Zimmermann, R. Gas chromatography in combination with fast high-resolution time-of-flight mass spectrometry: Technical overview and perspectives for data visualization. *TrAC, Trends Anal. Chem.* **2020**, *122*, 115677.
(31) Islam, A.; Cho, Y.; Ahmed, A.; Kim, S. Data interpretation methods for petroleomics. *Mass Spectrom. Lett.* **2012**, *3*, 63.
(32) Ridgeway, M. E.; Bleiholder, C.; Mann, M.; Park, M. A. Trends in trapped ion mobility − Mass spectrometry instrumentation. *TrAC, Trends Anal. Chem.* **2019**, *116*, 324.
(33) Cumeras, R.; Figueras, E.; Davis, C. E.; Baumbach, J. I.; Gràcia, I. Review on ion mobility spectrometry. Part 1: current instrumentation. *Analyst* **2015**, *140*, 1376−1390.
(34) Ahmed, A.; Cho, Y.; Giles, K.; Riches, E.; Lee, J. W.; Kim, H. I.; Choi, C. H.; Kim, S. Elucidating molecular structures of nonalkylated and short-chain alkyl ($n < 5$, $(CH_2)n$) aromatic compounds in crude oils by a combination of ion mobility and ultrahigh-resolution mass spectrometries and theoretical collisional cross-section calculations. *Anal. Chem.* **2014**, *86*, 3300.
(35) Lapthorn, C.; Pullen, F.; Chowdhry, B. Z. Ion mobility spectrometry-mass spectrometry (IMS-MS) of small molecules: separating and assigning structures to ions. *Mass Spectrom. Rev.* **2013**, *32*, 43.
(36) Ewing, M. A.; Glover, M. S.; Clemmer, D. E. Hybrid ion mobility and mass spectrometry as a separation tool. *J. Chromatogr. A* **2016**, *1439*, 3.
(37) Ujma, J.; Ropartz, D.; Giles, K.; Richardson, K.; Langridge, D.; Wildgoose, J.; Green, M.; Pringle, S. Cyclic Ion Mobility Mass Spectrometry Distinguishes Anomers and Open-Ring Forms of Pentasaccharides. *J. Am. Soc. Mass Spectrom.* **2019**, *30*, 1028.
(38) Farenc, M.; Paupy, B.; Marceau, S.; Riches, E.; Afonso, C.; Giusti, P. Effective Ion Mobility Peak Width as a New Isomeric Descriptor for the Untargeted Analysis of Complex Mixtures Using Ion Mobility-Mass Spectrometry. *J. Am. Soc. Mass Spectrom.* **2017**, *28*, 2476.
(39) Rüger, C. P.; Maillard, J.; Le Maître, J.; Ridgeway, M.; Thompson, C. J.; Schmitz-Afonso, I.; Gautier, T.; Carrasco, N.; Park, M. A.; Giusti, P.; Afonso, C. Structural Study of Analogues of Titan's Haze by Trapped Ion Mobility Coupled with a Fourier Transform Ion Cyclotron Mass Spectrometer. *J. Am. Soc. Mass Spectrom.* **2019**, *30*, 1169.
(40) Ropartz, D.; Fanuel, M.; Ujma, J.; Palmer, M.; Giles, K.; Rogniaux, H. Structure Determination of Large Isomeric Oligosaccharides of Natural Origin through Multipass and Multistage Cyclic Traveling-Wave Ion Mobility Mass Spectrometry. *Anal. Chem.* **2019**, *91*, 12030.
(41) Riches, E.; Palmer, M. E. Application of a novel cyclic ion mobility-mass spectrometer to the analysis of synthetic polymers: A preliminary evaluation. *Rapid Commun. Mass Spectrom.* **2020**, *34*, No. e8710.
(42) Kenderdine, T.; Nemati, R.; Baker, A.; Palmer, M.; Ujma, J.; FitzGibbon, M.; Deng, L.; Royzen, M.; Langridge, J.; Fabris, D. High-resolution ion mobility spectrometry-mass spectrometry of isomeric/isobaric ribonucleotide variants. *J. Mass Spectrom.* **2020**, *55*, e4465.
(43) Cho, E.; Riches, E.; Palmer, M.; Giles, K.; Ujma, J.; Kim, S. Isolation of Crude Oil Peaks Differing by m/z ∼ 0.1 via Tandem Mass Spectrometry Using a Cyclic Ion Mobility-Mass Spectrometer. *Anal. Chem.* **2019**, *91*, 14268.
(44) Bruns, E. A.; Perraud, V.; Greaves, J.; Finlayson-Pitts, B. J. Atmospheric solids analysis probe mass spectrometry: a new approach for airborne particle analysis. *Anal. Chem.* **2010**, *82*, 5922.
(45) Trimpin, S.; Clemmer, D. E. Ion mobility spectrometry/mass spectrometry snapshots for assessing the molecular compositions of complex polymeric systems. *Anal. Chem.* **2008**, *80*, 9073.
(46) Trimpin, S.; Plasencia, M.; Isailovic, D.; Clemmer, D. E. Resolving oligomers from fully grown polymers with IMS-MS. *Anal. Chem.* **2007**, *79*, 7965.
(47) Czech, H.; Miersch, T.; Orasche, J.; Abbaszade, G.; Sippula, O.; Tissari, J.; Michalke, B.; Schnelle-Kreis, J.; Streibel, T.; Jokiniemi, J.; Zimmermann, R. Chemical composition and speciation of particulate organic matter from modern residential small-scale wood combustion appliances. *Sci. Total Environ.* **2018**, *612*, 636.
(48) Chowdhury, P. H.; He, Q.; Carmieli, R.; Li, C.; Rudich, Y.; Pardo, M. Connecting the Oxidative Potential of Secondary Organic Aerosols with Reactive Oxygen Species in Exposed Lung Cells. *Environ. Sci. Technol.* **2019**, *53*, 13949.
(49) Chowdhury, P. H.; He, Q.; Lasitza Male, T.; Brune, W. H.; Rudich, Y.; Pardo, M. Exposure of Lung Epithelial Cells to Photochemically Aged Secondary Organic Aerosol Shows Increased Toxic Effects. *Environ. Sci. Technol. Lett.* **2018**, *5*, 424.
(50) Miersch, T.; Czech, H.; Hartikainen, A.; Ihalainen, M.; Orasche, J.; Abbaszade, G.; Tissari, J.; Streibel, T.; Jokiniemi, J.;

https://dx.doi.org/10.1021/jasms.0c00274
J. Am. Soc. Mass Spectrom. XXXX, XXX, XXX−XXX

Sippula, O.; Zimmermann, R. Impact of photochemical ageing on Polycyclic Aromatic Hydrocarbons (PAH) and oxygenated PAH (Oxy-PAH/OH-PAH) in logwood stove emissions. *Sci. Total Environ.* **2019**, *686*, 382.
(51) Peng, Z.; Day, D. A.; Stark, H.; Li, R.; Lee-Taylor, J.; Palm, B. B.; Brune, W. H.; Jimenez, J. L. HO x radical chemistry in oxidation flow reactors with low-pressure mercury lamps systematically examined by modeling. *Atmos. Meas. Tech.* **2015**, *8*, 4863.
(52) Peng, Z.; Day, D. A.; Ortega, A. M.; Palm, B. B.; Hu, W.; Stark, H.; Li, R.; Tsigaridis, K.; Brune, W. H.; Jimenez, J. L. Non-OH chemistry in oxidation flow reactors for the study of atmospheric chemistry systematically examined by modeling. *Atmos. Chem. Phys.* **2016**, *16*, 4283.
(53) Peng, Z.; Jimenez, J. L. Modeling of the chemistry in oxidation flow reactors with high initial NO. *Atmos. Chem. Phys.* **2017**, *17*, 11991.
(54) Schwemer, T.; Rüger, C. P.; Sklorz, M.; Zimmermann, R. Gas Chromatography Coupled to Atmospheric Pressure Chemical Ionization FT-ICR Mass Spectrometry for Improvement of Data Reliability. *Anal. Chem.* **2015**, *87*, 11957.
(55) Giles, K.; Ujma, J.; Wildgoose, J.; Pringle, S.; Richardson, K.; Langridge, D.; Green, M. A Cyclic Ion Mobility-Mass Spectrometry System. *Anal. Chem.* **2019**, *91*, 8564.
(56) Rüger, C. P.; Schwemer, T.; Sklorz, M.; O'Connor, P. B.; Barrow, M. P.; Zimmermann, R. Comprehensive chemical comparison of fuel composition and aerosol particles emitted from a ship diesel engine by gas chromatography atmospheric pressure chemical ionisation ultra-high resolution mass spectrometry with improved data processing routines. *Eur. J. Mass Spectrom.* **2017**, *23*, 28.
(57) Altgelt, K. H.; Boduszynski, M. M. Composition of heavy petroleums. 3. An improved boiling point-molecular weight relation. *Energy Fuels* **1992**, *6*, 68.
(58) Boduszynski, M. M. Composition of heavy petroleums. 1. Molecular weight, hydrogen deficiency, and heteroatom concentration as a function of atmospheric equivalent boiling point up to 1400 °F (760 °C). *Energy Fuels* **1987**, *1*, 2.
(59) Boduszynski, M. M. Composition of heavy petroleums. 2. Molecular characterization. *Energy Fuels* **1988**, *2*, 597.
(60) Boduszynski, M. M.; Altgelt, K. H. Composition of heavy petroleums. 4. Significance of the extended atmospheric equivalent boiling point (AEBP) scale. *Energy Fuels* **1992**, *6*, 72.
(61) Rüger, C. P.; Sklorz, M.; Schwemer, T.; Zimmermann, R. Characterisation of ship diesel primary particulate matter at the molecular level by means of ultra-high-resolution mass spectrometry coupled to laser desorption ionisation-comparison of feed fuel, filter extracts and direct particle measurements. *Anal. Bioanal. Chem.* **2015**, *407*, 5923.
(62) Streibel, T.; Schnelle-Kreis, J.; Czech, H.; Harndorf, H.; Jakobi, G.; Jokiniemi, J.; Karg, E.; Lintelmann, J.; Matuschek, G.; Michalke, B.; Muller, L.; Orasche, J.; Passig, J.; Radischat, C.; Rabe, R.; Reda, A.; Ruger, C.; Schwemer, T.; Sippula, O.; Stengel, B.; Sklorz, M.; Torvela, T.; Weggler, B.; Zimmermann, R. Aerosol emissions of a ship diesel engine operated with diesel fuel or heavy fuel oil. *Environ. Sci. Pollut. Res.* **2017**, *24*, 10976.
(63) Marshall, A. G.; Rodgers, R. P. Petroleomics: chemistry of the underworld. *Proc. Natl. Acad. Sci. U. S. A.* **2008**, *105*, 18090.
(64) Eichler, P.; Müller, M.; Rohmann, C.; Stengel, B.; Orasche, J.; Zimmermann, R.; Wisthaler, A. Lubricating Oil as a Major Constituent of Ship Exhaust Particles. *Environ. Sci. Technol. Lett.* **2017**, *4*, 54.
(65) Worton, D. R.; Isaacman, G.; Gentner, D. R.; Dallmann, T. R.; Chan, A. W. H.; Ruehl, C.; Kirchstetter, T. W.; Wilson, K. R.; Harley, R. A.; Goldstein, A. H. Lubricating oil dominates primary organic aerosol emissions from motor vehicles. *Environ. Sci. Technol.* **2014**, *48*, 3698.
(66) Kalberer, M.; Paulsen, D.; Sax, M.; Steinbacher, M.; Dommen, J.; Prevot, A. S. H.; Fisseha, R.; Weingartner, E.; Frankevich, V.; Zenobi, R.; Baltensperger, U. Identification of Polymers as Major Components of Atmospheric Organic Aerosols. *Science* **2004**, *303*, 1659.
(67) Rhead, M. M.; Hardy, S. A. The sources of polycyclic aromatic compounds in diesel engine emissions. *Fuel* **2003**, *82*, 385.
(68) Orasche, J.; Seidel, T.; Hartmann, H.; Schnelle-Kreis, J.; Chow, J. C.; Ruppert, H.; Zimmermann, R. Comparison of Emissions from Wood Combustion. Part 1: Emission Factors and Characteristics from Different Small-Scale Residential Heating Appliances Considering Particulate Matter and Polycyclic Aromatic Hydrocarbon (PAH)-Related Toxicological Potential of Particle-Bound Organic Species. *Energy Fuels* **2012**, *26*, 6695.
(69) Sippula, O.; Stengel, B.; Sklorz, M.; Streibel, T.; Rabe, R.; Orasche, J.; Lintelmann, J.; Michalke, B.; Abbaszade, G.; Radischat, C.; Gröger, T.; Schnelle-Kreis, J.; Harndorf, H.; Zimmermann, R. Particle emissions from a marine engine: chemical composition and aromatic emission profiles under various operating conditions. *Environ. Sci. Technol.* **2014**, *48*, 11721.
(70) Di Filippo, P.; Pomata, D.; Riccardi, C.; Buiarelli, F.; Gallo, V. Oxygenated polycyclic aromatic hydrocarbons in size-segregated urban aerosol. *J. Aerosol Sci.* **2015**, *87*, 126.
(71) Lewtas, J. Air pollution combustion emissions: characterization of causative agents and mechanisms associated with cancer, reproductive, and cardiovascular effects. *Mutat. Res., Rev. Mutat. Res.* **2007**, *636*, 95.
(72) Xue, W.; Warshawsky, D. Metabolic activation of polycyclic and heterocyclic aromatic hydrocarbons and DNA damage: a review. *Toxicol. Appl. Pharmacol.* **2005**, *206*, 73.
(73) Hartikainen, A.; Tiitta, P.; Ihalainen, M.; Yli-Pirilä, P.; Orasche, J.; Czech, H.; Kortelainen, M.; Lamberg, H.; Suhonen, H.; Koponen, H.; Hao, L.; Zimmermann, R.; Jokiniemi, J.; Tissari, J.; Sippula, O. Photochemical transformation of residential wood combustion emissions: dependence of organic aerosol composition on OH exposure. *Atmos. Chem. Phys.* **2020**, *20*, 6357.

https://dx.doi.org/10.1021/jasms.0c00274
J. Am. Soc. Mass Spectrom. XXXX, XXX, XXX−XXX